Fusion Engineering and Design 215 (2025) 115046

Contents lists available at ScienceDirect

Fusion Engineering and Design

journal homepage: www.elsevier.com/locate/fusengdes

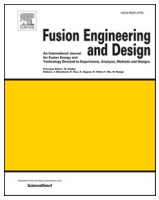

Insight into the structural integrity assessment of the European DEMO fusion reactor divertor (Part II: Application examples)

M. Muscat [a,*], P. Mollicone [a], N. Mantel [b], J.H. You [c], C. Carrelli [d], A. Aleksa [b], J. Hess [b]

[a] Department of Mechanical Engineering, Faculty of Engineering, University of Malta, Malta
[b] UKAEA (United Kingdom Atomic Energy Authority), Culham Campus, Abingdon, Oxfordshire OX14 3DB, UK
[c] IPP (Max Planck Institute for Plasma Physics), Garching, Germany
[d] ENEA (Italian National Agency for New Technologies, Energy and Sustainable Economic Development), Brasimone, Italy

ARTICLE INFO

Keywords:
Fusion reactors
DEMO
Divertor
RCC-MRx
Structural integrity
Elastic analysis

ABSTRACT

The DEMO fusion reactor Divertor design group within the EUROfusion consortium use RCC-MRx as the main analysis code for the Divertor's structural integrity assessment. Analysis has been carried out within the same group using an in-house developed Finite Element Analysis post processing script which follows the Design by Elastic Analysis rules of RCC MRx. A number of stress classification lines (SCLs) were placed in the Divertor component regions which are susceptible to Type P and Type S damage. This paper focuses on two of these stress classification lines. One is located in the region of a stress singularity while the other is in a region of high stress where the temperature is above the creep threshold along part of the SCL. Design by Analysis was performed using a spreadsheet application. The purpose was to highlight difficulties encountered in using the RCC-MRx elastic design methodology applied to the DEMO divertor. Issues mainly arose because of stress singularities in the geometry, because of the inherent non-axisymmetric geometry and loading of the divertor and because of limited material data for Eurofer97 steel which is the main material used for the DEMO Divertor. This paper is Part II of a companion paper and compliments it by considering the two SCLs as application examples and case studies. In the companion paper (Part I), general discussions on the difficulties and issues encountered are presented including some theoretical background on the phenomenon of elastic follow up and on Neuber's hyperbola rule that addresses plasticity and stress relaxation. An additional outcome of this work emphasises the need to further develop the in-house Finite Element Analysis post processing script and to incorporate within it best practice in implementing the RCC-MRx Design by Elastic Analysis rules for the Divertor components. The post processing tool development would improve the assessment reliability and productivity in order to suggest timely Divertor design modifications.

1. Introduction

In the DEMO fusion reactor, in-vessel components will be subjected to very high thermo mechanical steady and cyclic loads. Currently the WP DIV group uses the DBA elastic route of the RCC MRx code of standard [1] to perform structural integrity checks on the divertor components [2–4]. The design of one of the latest models of the DEMO divertor is shown in Fig. 1. This divertor model is referred to as the 'Dual circuit' single null DEMO Divertor model [5]. The elastic DBA methodologies in RCC MRx are summarised in [6]. In essence, these rules prevent failure due to monotonic and cyclic loads including temperature loading under non-irradiated and irradiated conditions. RCC MRx was primarily written for fission nuclear reactors in which normally the fission reactor's pressurised component has an axisymmetric geometry and is acted upon by axisymmetric loadings. In a nuclear fusion reactor, the geometry of the high temperature components, such as that of the divertor, is far from being axisymmetric both in geometry and loading. The geometry is of a box type (Fig. 1) and for these types of structures the code [1] does not give much guidance for performing stress classification especially in regions of stress concentration. This raises issues and queries on the applicability of some sections of the RCC MRx RB 3200 Design by elastic analysis approach used to assure the structural integrity of the DEMO Divertor components.

This paper highlights some of these code sections by considering

* Corresponding author.
E-mail address: martin.muscat@um.edu.mt (M. Muscat).

https://doi.org/10.1016/j.fusengdes.2025.115046
Received 15 October 2024; Received in revised form 13 March 2025; Accepted 2 April 2025
Available online 9 April 2025

specific stress classification lines (SCLs) taken from references [2] and [3]. References [2] and [3] use the DBA elastic analysis approach to perform a structural integrity assessment of the divertor components by placing stress classification lines (SCLs) in identified regions susceptible to Type P and Type S damage under the given load cases including thermal loading. The authors for this paper select two of these SCLs that are as much as possible near to a stress singularity and that are near to an area of high stress where the temperature through the thickness is above the creep temperature. The first SCL that is selected is in the cassette near to (but not at) a stress singularity and in an area where the temperature is below the threshold for creep. The second SCL that is selected is in the shielding liner far from a stress singularity but in an area where part of the SCL is above the threshold creep temperature.

Results from calculations performed by the authors using a spreadsheet program are compared with results from the in-house developed finite element analysis post processing script [7] and presented in [2] and [3]. The script is run as a postprocessing tool in Ansys® Academic Research Mechanical 2023R2 [8]. In general, the main problems encountered in applying the rules are connected to regions of geometrical discontinuities, to lack of irradiated material properties and to the RCC MRx code rule interpretation as applied to the DEMO Divertor components which have a box type of structure. The code rules for such type of structures may be interpreted differently by different stress analysts so that more guidelines for best practice must be further developed. The divertor cassette is above the negligible irradiation level and so this raises serious concerns in being able to perform design checks under irradiated conditions. The current dual circuit model of the DEMO divertor has a number of geometrical discontinuities at which it is not possible to determine the stress value. This means that checks that require the total stress at a stress singularity are not possible unless a method is developed to deal with such stress singularities.

For the negligible creep tests (RB 3216.1), the negligible creep curve in A3.31 [1] is not yet available for Eurofer97 steel so that part of these tests could not be carried out. Not having the negligible creep curve available can make the assessment more conservative in case of high temperatures.

References [2,3] give the structural integrity results based on RCC MRx rules for the pre-load assessment on the wishbone geometry acted upon by an SL1 and SL2 seismic and Electromagnetic (EM) loading and for the DEMO Divertor cassette under Normal operating condition (NOC), seismic loading (SL1), Pressure test, Baking and electromagnetic (EM) loading. Table 1 shows the load steps applied to the DEMO divertor cassette including the shielding liner and the reflector plates. A value of '1′ in Table 2 indicates that the type of load shown in the column heading is applied while a value of '0′ indicates that load is not applied for a specific load case. For the 'Temperature' column and load cases 1 to 4 the 'Thermal map' is the temperature field obtained from other Computational fluid dynamics (CFD) and thermal analyses. The thermal map for the DEMO divertor cassette for load cases 1 to 4 is shown in Fig. 2. For load cases 5 to 12 the temperature field is constant for the whole divertor model at the value shown.

Table 2 shows the elastic solution combinations used to evaluate the primary stresses at every operating condition, by subtracting the secondary stress field from the primary plus secondary stress field. This is an efficient way of determining the primary stress fields without having to re-run the FE solutions with the temperature loading removed by setting the coefficient of thermal expansion to zero.

Here it must be noted that as a first iteration, stresses are deemed secondary if they are the result of temperature loading. Discontinuity stresses at junctions and preload induced stresses are assumed to be primary which would result in a conservative design unless elastic follow up takes place. It is planned that for future design improvements, discontinuity stresses at junctions will be considered as secondary or local primary membrane. Having said that, not much guidance is given in codes of standard on how to classify stresses (especially local and membrane stresses) at junctions for box type of structures.

Table 3 gives the number of cycles for a number of load cases which were used for a fatigue assessment [2,3]. For EM, SL1 and for the pressure test load cases, the assessment was carried out for one cycle only due to lack of data on the number of events connected to these particular load cases. However, this will act as a guide to the designers to understand the fatigue life fraction consumed by each event. In addition, the duration of baking is not accounted for as this is only required for a creep calculation and the baking temperature for most SCLs is below the negligible creep temperature for Eurofer97 steel [2,3]. The same can be said for the duration of the pressure test. The duration for the EM and SL1 load cases is not yet available but it is envisaged that these will be short term events so that creep strains will not have enough time to build up. Having said that, the latter load durations would allow the stress analysts to check for creep during these loading events.

The in-house developed finite element analysis post processing script considers stress results along paths (SCLs) drawn through the wall thickness of the components in relevant regions. The SCLs are defined manually by the analysts. The stress results are linearised along the SCLs and categorised into membrane stress, bending stress and total stress using the software's stress linearisation capabilities. The latter linearise all the stress tensor components and are in line with the stress linearisation equations of RCC-MRx [1]. In the region of stress singularities, it is stated in [2] and [3] that the SCLs were positioned at least two or three elements away from the singularity. In such a situation it must be ensured that the mesh is fine enough to result in a converged stress field. Since the divertor components are subjected to an uneven temperature

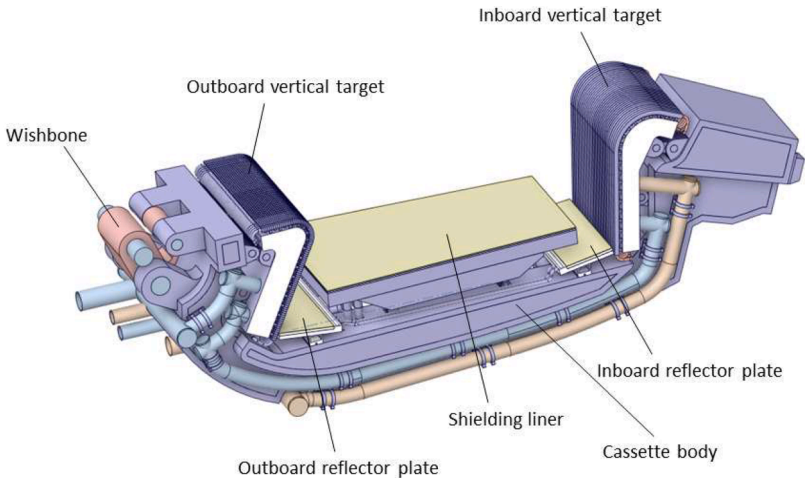

Fig. 1. The main components of one of the latest DEMO divertor design.

Table 1
Load cases for different loading scenarios.

Load case	Description	Displacement	Temperature	Pressure	SL1	Ferro Magnetic	EM	Gravity
1	NOC EM SL1 Secondary stress	0	Thermal map	0	0	0	0	0
2	NOC Primary + secondary stress	1	Thermal map	3.5MPa	0	1	0	1
3	EM Primary + secondary stress	1	Thermal map	3.5MPa	0	1	1	1
4	SL1 Primary + secondary stress	1	Thermal map	3.5MPa	1	1	0	1
5	Baking case Secondary stress	0	240 °C	0	0	0	0	0
6	Baking case Primary + Secondary stress	1	240 °C	3.5MPa	0	0	0	1
7	Pressure test Secondary stress	0	130 °C	0	0	0	0	0
8	Pressure test Primary + secondary stress	1	130 °C	6MPa	0	0	0	1
9	Dwell Secondary	0	180 °C	0	0	0	0	0
10	Dwell Primary + secondary stress	1	180 °C	3.5MPa	0	1	0	1
11	As installed secondary	0	20 °C	0	0	0	0	0
12	As installed Primary + secondary stress	1	20 °C	0	0	0	0	1

Table 2
Load combinations to calculate primary stresses.

Load step combination	Description	Operation on load step
1	NOC Primary	Subtract Load step 1 from load step 2
2	EM Primary	Subtract Load step 1 from load step 3
3	SL1 Primary	Subtract Load step 1 from load step 4
4	Baking Primary	Subtract Load step 5 from load step 6
5	Pressure test Primary	Subtract Load step 7 from load step 8
6	Dwell Primary	Subtract Load step 9 from load step 10
7	As installed Primary	Subtract Load step 11 from load step 12

distribution during plasma operations, most regions for stress linearisation were selected by plotting the maximum von Mises stress intensity over all load cases normalised over the yield stress function of Eurofer97 steel at the respective temperature. Such a contour plot is shown in Fig. 3.

Results of the assessment in [2] and [3] are printed as outcome of the finite element post processing script, showing the factor of safety against all specific RCC-MRx assessment for each SCL in the model. In [7] the creep check was considered applicable if the maximum temperature over the path was above 375 °C, which is the threshold temperature for creep to occur in Eurofer97 steel. In the case of the Type P checks and the Type S progressive deformation check this is conservative if the average temperature over the SCL is below the creep threshold temperature. This is because the plastic instability and excessive deformation checks seek failure across the entire structural wall cross section. Similarly, the progressive deformation check has to do with global overall expanding movement of the wall of the box structure while the load is cycling rather than an increase in the local strain value. This is in contrast with the fatigue and creep fatigue checks which address failure at a local point on the SCL so that for the latter case all material properties and checks including the negligible creep check need to be carried out at the local maximum temperature reached at the point under consideration.

Reference [2] reported that for the pre-load assessment on the cassette and wishbone there was no loss of pre-load under the SL1 load case. A pre-load applied through the wishbone acting as a large spring is required to secure the divertor cassette in place within the vacuum vessel. During the work carried out in [2] there was insufficient data

Table 3
Fatigue cycle definitions.

Cycle ID	Cycle definition	Number of cycles	Length of time for which load is acting
Plasma pulse	NOC / Dwell	6859 [6]	2 h
Baking	Baking / As installed	2 for 3 full power years (Fpy)	N/A
EM	Vertical displacement event (VDE) / Dwell	1	N/A
SL1	SL1 / Dwell	1	N/A
Pressure test	Pressure test / As installed	1	N/A

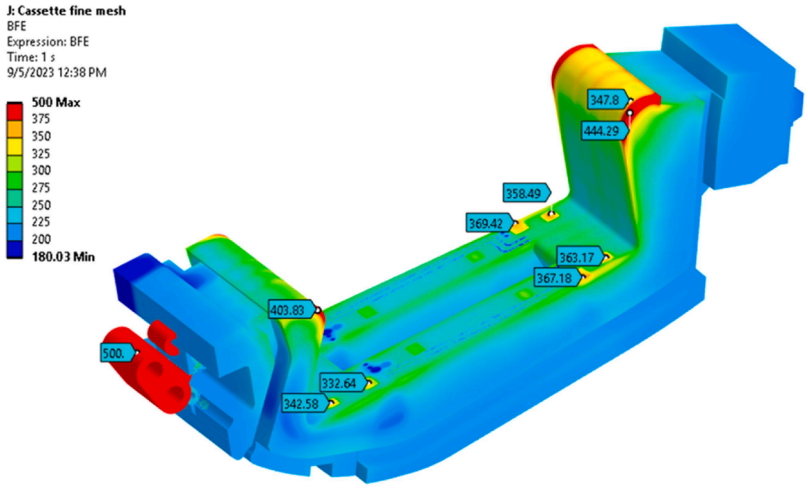

Fig. 2. The thermal map for the DEMO divertor cassette for load case 1. The shielding liner and reflector plates are removed for clarity.

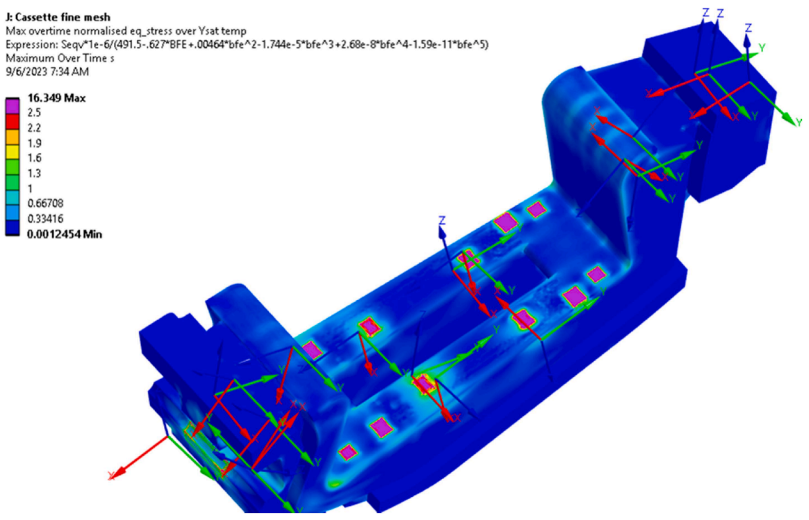

Fig. 3. von Mises stress intensity divided by the yield stress at the local temperature.

available on the plastic material behaviour to assess wishbone pre-load for the NOC load case. The material selected for the wishbone is Titanium 318. The elastic analysis revealed that part of the wishbone would behave plastically and this would affect the pre-load on the cassettes. Further work on the wishbone analysis was therefore recommended. The stresses induced in the cassette by the wishbone were deemed to be primary since the wishbone acts as a spring so that the phenomenon of elastic follow up is deemed to take place. Having said that, no thorough analysis was carried out in [2] to determine the elastic follow up factor and so reduce the conservative assumption that the wishbone stresses are wholly primary.

Under the SL2 load case all preload on the cassette was lost [2]. SL2 is classified as a category 4 (SF4) event [1]. This category of loading is highly improbable to occur but never-the-less should be analysed to prevent damage done to the in-vessel components and to the vacuum vessel itself in case a cassette or some other component suffer a loss of restraint event.

Analyses did not consider the effect of welds on material properties [2,3]. These must be considered in future analyses [1] once the fabrication method for the DEMO divertor cassette is known.

Reference [2] gives further details on results for the DEMO divertor cassette. Under the action of the given load cases not all SCLs satisfied the Type P and Type S checks. This suggests the need for design changes. Most Type P failure occurred for the NOC load case. EM and SL1 load cases did not contribute a significant amount to the overall damage factor. It must be noted that the EM loading was not being properly applied to the finite element model because of a mismatch in geometries between the EM model and the Mechanical model. This will be addressed in future work. Fatigue Type S assessment due to cyclic loading was only carried out for the NOC load case [3].

Results given in [3] show that none of the shielding liner or reflector plates satisfied all the RCC-MRx elastic design rules. This again suggested the need for design changes. Fatigue during NOC appears to be a particular issue with only one result meeting the allowable limits.

2. Detailed structural integrity assessment for the NOC load case for the SCL in the region of a stress singularity

References [2] and [3] indicate that the worst loading conditions that were included in the analysis occurred during the NOC load case. The NOC load case is given as load case 2 in Table 1. This section therefore considers the required calculations for the NOC load case (for a SCL in the region of a stress singularity) and draws comparison with the previous post processing script results. Fig. 4 shows the position and orientation of the SCL within the DEMO divertor cassette.

The temperature along the chosen SCL is below the threshold creep temperature for Eurofer97. Fig. 5 shows a von Mises stress plot near the region of the SCL including the nearby stress singularity area for load case 2 which is the NOC load case. The stress classification line under consideration is labelled as SCL 10.

2.1. Primary, secondary and total stresses – stress linearization and categorisation

2.1.1. Load case 2 – primary and secondary stresses - normal operating load case (NOC)

Fig. 6 shows the variation through the thickness of the Primary + Secondary stress for SCL 10 for Load case 2 (NOC). The NOC load case includes the thermal load, 3.5 MPa cooling water pressure, the ferromagnetic load and the effect of gravity.

2.1.2. Load combination 1 - primary stress through thickness for SCL 10 for load case 2 (NOC)

Fig. 7 shows the Primary stress through thickness for SCL 10 for Load case 2 (NOC). This was obtained by using load combinations in ANSYS Mechanical by subtracting the Thermal secondary stress field (Load Case 1) from the Primary plus Secondary stress field [2,3].

2.1.3. Comments on stress linearization at SCL 10 (region of stress singularity)

The stress classification line (SCL 10) under consideration is in the vicinity of a stress singularity, precisely 42 mm away from the

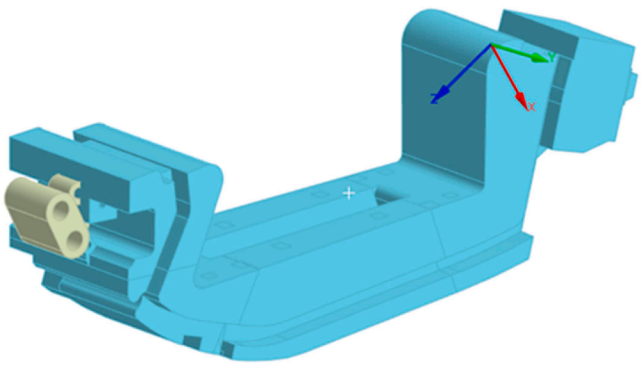

Fig. 4. Position and orientation of the coordinate system of the SCL under consideration.

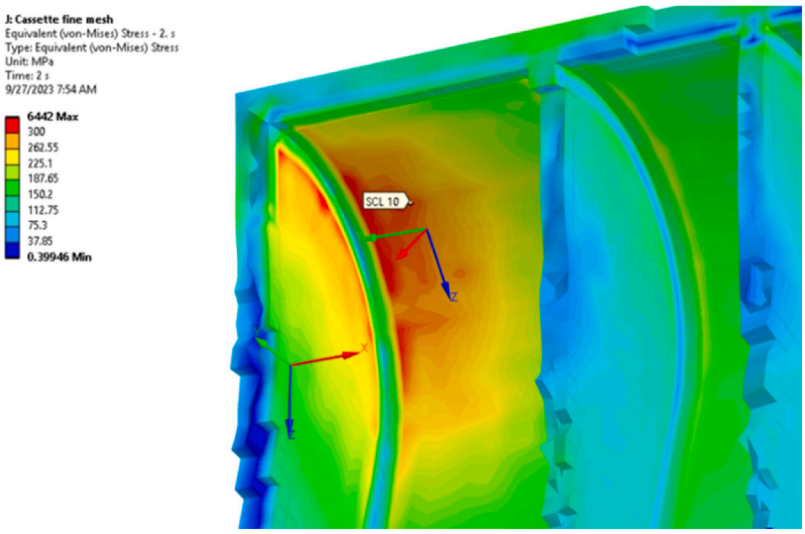

Fig. 5. Load case 2: NOC Secondary + Primary stresses (includes Thermal load, 3.5 MPa pressure, Ferromagnetic & Gravity).

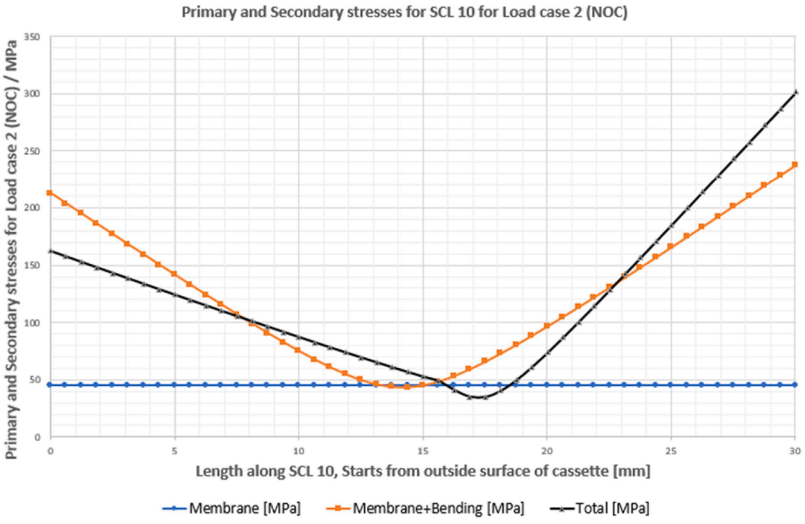

Fig. 6. Primary + Secondary stresses through thickness for SCL 10 for Load case 2 (NOC).

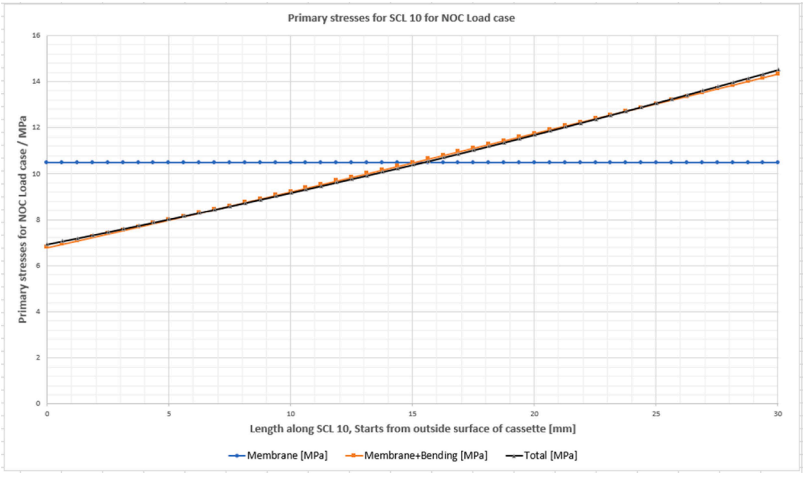

Fig. 7. Primary stress through thickness for SCL 10 for Load case 2 (NOC).

singularity, which happens to be 1.4 × the wall thickness of 30 mm at the point. This distance away from the singularity is that used in the hot spot method to evaluate the fatigue life of welded material by surface stress extrapolation [9].

Therefore, based on the latter, it can be hypothesised that SCL 10 is far enough from the junction so that at that location there is no stress singularity. Note, how, when the secondary stress field is removed from the Primary + Secondary stress field, the resulting total stress distribution is very similar to the Membrane + Bending stress distribution, Fig. 7. This occurs since SCL 10 is not situated at a stress concentration or stress singularity and the non-linearity is only due to thermal stresses. This demonstrates the effectiveness of stress linearization to separate the nonlinear thermal stresses from the Membrane + Bending stresses.

As can be seen in Fig. 6, contrary to what one would expect, the total stress on the outside surface is lower than the membrane + bending stress. This also happens at stress component level and the authors attribute it partly to the thermal stresses as discussed in the 'Guidelines for the selection of stress classification lines' in the ASME Boiler and Pressure vessel code, Section VIII, Division 2 [10]. Another reason may be the type of loading particular to fusion reactors. Probably this is a case that needs assessment using an elastic plastic approach in order to check on the validity of the elastic approach to DBA for such components.

For this report, the membrane, membrane + bending and total stresses are used as defined in RCC MRx [1] and as given in the ANSYS Mechanical result output. For 3D cartesian FE models, RCC-MRx uses the same linearization equations as those used in ANSYS Mechanical. This means that the stress linearization procedures programmed in ANSYS Mechanical can be used directly when following RCC-MRx rules for elastic DBA and the results used directly to compare with allowables.

2.1.4. Table of linearised stresses, total and cyclic stresses for SCL 10 and load case NOC

Table 4 shows the linearised, total and cyclic stresses for SCL 10 used in the RCC MRx assessment. For Membrane plus Bending and for Total stresses, both values on the inside and outside surfaces along SCL 10 are being shown. Similarly details such as temperature and temperature ranges at the point are also shown. The stress categories shown in column 1 are as those defined by RCC-MRx [1] and all the stress values are obtained from the finite element model for the divertor cassette. Some of these stresses have been shown in more detail in Sections 2.1.1 and 2.1.2 in this paper.

2.1.5. Summary of results from reference [2] for SCL10 (NOC load case)

Fig. 8 shows the results for SCL 10 as obtained from [2] which utilised the finite element post processing script. The purpose of the next sections will be to perform a structural integrity assessment for SCL 10 following RCC-MRx, comparing the results with those shown in Fig. 8 for the NOC Load case and as a consequence discuss difficulties and issues encountered in code interpretation and implementation to perform a structural integrity assessment of the DEMO divertor cassette.

2.2. Creep, irradiation and ageing checks

2.2.1. The negligible creep test - RB 3216.1

Since the temperature along SCL 10 is everywhere below 375 °C the rules for negligible creep (RB 3251 Type P damage and RB 3261 Type S damage) have been followed.

2.2.2. Irradiation & ageing tests - RB 3216.2 & RB 3216.3 [1]

Irradiation and aging have not been considered so that rules for negligible irradiation RB 3251.1 for Type P damage and RB 3261.111 to RB 3261.113 for Type S damage Progressive Deformation and Fatigue are followed respectively [1].

2.3. Preventing type P damages - negligible creep & negligible irradiation - RB 3251.1 – level A criteria

The Type P check addresses failure due to plastic instability and excessive deformation so that failure modes are associated with the global failure or excessive deformation over the entire structural wall thickness. This requires using the material properties calculated at the mean wall temperature θ_m.

Table 5 shows the numerical data required while Table 6 shows the comparison of stresses with their respective allowables for the Type P check. In Table 6, $S_m(\theta_m)$ is the allowable stress given in A3.43 [1] at the mean temperature θ_m (310.46 °C) calculated along the SCL. Using Table A3.19AS.41 probationary rules and linear interpolation, for Eurofer97 steel [1] the value for S_m at 310.46 °C is calculated to be 190.12 MPa.

The conclusion from Table 6 is that all the allowable stresses for the Type P check are satisfied for the stress classification line under consideration (SCL10).

2.4. Preventing type S damages - negligible creep & negligible irradiation - RB 3261.111 & RB 3261.113 – level A criteria

2.4.1. The normal operation NOC / dwell cycle

During the NOC load case the loads being applied are the thermal map load, the cooling water pressure, the ferromagnetic, and earth gravity.

During the Dwell load case the loads being applied are the thermal

Table 4
Linearised stresses for SCL 10 used in the structural integrity assessment (Load case NOC).

	Temperature °C	Membrane MPa	Membrane ± Bending MPa		Total MPa	
Secondary	T_{inside} = 230.44	42.32	236.5	212.56	300.39	161.88
NOC	$T_{outside}$ = 347.84		(Inside)	(Outside)	(Inside)	(Outside)
Primary ± Secondary	T_{inside} = 230.44	44.87	237.4	212.56	301.4	(Outside)
NOC	$T_{outside}$ = 347.84		(Inside)	(Outside)	(Inside)	162.29
Primary	T_{inside} = 230.44	10.47	14.317	6.795	14.51	6.931
NOC	$T_{outside}$ = 347.84		(Inside)	(Outside)	(Inside)	(Outside)
$\overline{\Delta Q}$	ΔT_{inside} = (230.44 −180) $\Delta T_{outside}$ = (347.84 −180)	42.86	236.61	212.7	300.53	162.11
NOC/Dwell			(Inside)	(Outside)	(Inside)	(Outside)
$\overline{\Delta Q}$	ΔT_{inside} = (230.44 −20) $\Delta T_{outside}$ = (347.84 −20)	42.29	236.48	212.54	300.37	161.85
NOC/As installed			(Inside)	(Outside)	(Inside)	(Outside)
$\overline{\Delta\sigma_{tot}} = \overline{\Delta(P+Q+F)}$	ΔT_{inside} = (230.44 −20) $\Delta T_{outside}$ = (347.84 −20)	45.12	237.47	212.55	301.47	162.36
For fatigue assessment NOC/As installed			(Inside)	(Outside)	(Inside)	(Outside)
$\overline{\Delta\sigma_{tot}} = \overline{\Delta(P+Q+F)}$	ΔT_{inside} = (230.44 −180) $\Delta T_{outside}$ = (347.84 −180)	43.39	236.97	213.01	300.93	162.52
For fatigue assessment NOC/Dwell			(Inside)	(Outside)	(Inside)	(Outside)

Table 32: Path 10 assessment results

Results over Path 10	NOC	EM	SL1	Baking	Pressure test
Creep Check	N/A	N/A	N/A	N/A	N/A
TypeP Assessment	TRUE	True	True	True	True
Type P Membrane	18.16	9.61	18.26	325.49	264.26
Type P Membrane + Bending	19.73	10.51	19.82	332.72	271.78
TypeS Assessment :	FALSE	True	True	True	True
Type S Ratcheting Membrane	2.66	2.50	2.66	172.91	274.50
Type S Ratcheting Membrane + Bending	2.44	2.36	2.44	207.89	310.75
Type S Fatigue Usage	5.91	0.00	0.00	0.00	0.00
Type S Fatigue Usage %	590.77%	0.10%	0.09%	0.08%	0.02%

Fig. 8. Summary of results for SCL 10 from reference [2].

Table 5
Numerical Data required for the Type P check.

Parameters:	Definition:	Value: (From Table 4)
$\overline{P_m}$	General primary membrane stress intensity	10.47 MPa
$\overline{P_L}$	Local primary membrane stress intensity	10.47 MPa
$\overline{P_L + P_b}$	Primary membrane plus bending stress intensity	14.32 MPa

Table 6
Comparison of stresses for the Type P check.

Stress allowables:	Notes:	S_m=190.12 MPa
$\overline{P_m} \leq S_m(\theta_m)$	SCL 10 far away from a gross, local or geometric discontinuity	$\overline{P_m}$ = 10.47 MPa < S_m Allowable is satisfied
$\overline{P_L} \leq 1.5.S_m(\theta_m)$	SCL 10 far away from a gross, local or geometric discontinuity so that $\overline{P_L} = \overline{P_m}$	$\overline{P_L}$ = 10.47 MPa < 1.5S_m Allowable is satisfied
$\overline{P_L + P_b} \leq 1.5.S_m(\theta_m)$	SCL 10 far away from a gross, local or geometric discontinuity	$\overline{P_L + P_b}$ = 14.32 MPa < 1.5S_m Allowable is satisfied

load at 180 °C uniform temperature, the cooling water pressure, the ferromagnetic and earth gravity.

Therefore, the cyclic load is the secondary one and is due to thermal cycling between the NOC temperature distribution and the Dwell 180 °C uniform temperature distribution. Table 7 gives the required values for the primary membrane, the primary membrane plus bending stresses and the cyclic stress range.

For the progressive deformation check the maximum mean temperature over the cycle is used in order to calculate the required material properties. This is so since progressive deformation failure is related to the global ratchetting failure of the structural wall. On the other hand, the fatigue check requires the local temperature to be used for calculating the required material properties since fatigue failure is a local type of failure. Membrane plus bending ($M + B$) and total stresses are used for the progressive deformation check and for the fatigue check respectively for the same reasons.

Table 4 for the NOC secondary stress category shows that there is a secondary membrane stress of 42.32 MPa so that the RCC-MRx progressive deformation check rules followed are those associated with the 'Special case for structures that present secondary membrane stress'. It must be also noted that to calculate Max. $\overline{P_L + P_b + Q_m}$ the addition between $\overline{P_L + P_b}$ and $\overline{Q_m}$ must be carried out at stress tensor component level and the von Mises stress is then calculated. Table 7 shows the required parameters for the progressive deformation and fatigue checks.

2.4.2. The progressive deformation failure check

The normal operation NOC load case is a case without overload of short duration therefore the rules in RB 3261.1112 [1] are followed. Gamma type of heating was included in the thermal map in the FE model [2]. Having said this, the specific case for Gamma heating which results in a highly non-linear temperature distribution throughout the thickness was not followed. The decision on a non linear temperature distribution resulting in high thermal gradient across the wall thickness is deemed by the authors to be a subjective decision and this was left for future analysis. As has been mentioned previously, the NOC load case is a situation of secondary membrane stress Q_m. Therefore, the equations that follow are used [1].

$$\mathbf{Max}(\sigma_m) = \frac{1}{2}[Max(\overline{P_m}) + (\sigma_m)_N] \tag{1}$$

$$\mathbf{Max}(\sigma_L + \sigma_b) = \frac{1}{2}[Max(\overline{P_L + P_b}) + (\sigma_L + \sigma_b)_N] \tag{2}$$

$$\Delta q = \overline{\Delta Q} \tag{3}$$

where

$(\sigma_m)_N$ is the stress obtained after applying Neuber's rule to Max $\overline{P_m + Q_m}$ as shown in the RCC-MRx Figure RB 3261.1111a which is Fig. 9a in this paper.

$(\sigma_L + \sigma_b)_N$ is the stress obtained after applying Neuber's rule to Max $\overline{P_L + P_b + Q_m}$ as shown in the RCC-MRx Figure RB 3261.1111b which is Fig. 9b in this paper.

The minimum tensile curves for Eurofer97 are given by formula A3.19AS.451b [1]:

$$\varepsilon_t = 100\frac{\sigma}{E} + \left[\frac{\sigma}{(C_o \times (R_{p0.2\ min}))}\right]^{\frac{1}{n_o}} \tag{4}$$

in which the Young's Modulus, E, is calculated to be 201,342 MPa at the mean temperature of 310.46 °C. Refer to A3.22 for Eurofer97 steel [1]. Consequently ε at $\overline{P_m + Q_m} = 44.87\ MPa$ is given by $\varepsilon = \frac{\overline{P_m + Q_m}}{E} = \frac{44.87}{201342} = 2.2285 \times 10^{-4} = 0.022285$%

Therefore the constant for Neuber's rule $= \sigma\varepsilon = 44.87 \times 0.022285 = 0.99993$

In addition $R_{p0.2\ min}$ is given in A3.41 [1] as a function of temperature and is calculated to be 430.97 MPa at the mean temperature of 310.46 °C. The constants C_o and n_o are determined using linear interpolation at the same mean temperature.

Consequently the intersection between the minimum tensile curve at $\theta = 310.46^oC$ and Neuber's hyperbola results in $(\sigma_m)_N = 44.87\ MPa$.

Table 7
Numerical data used for the Progressive deformation and Fatigue checks.

Parameters:	Definition:	Value: (From Table 4)
Max. θ_m	Max. value of the mean temp. through the thickness	310.46 °C
Max. $\overline{P_m}$	Max. value of the primary membrane stress intensity	10.47 MPa
Max. $\overline{P_L + P_b}$	Max. value of the primary membrane plus primary bending stress intensity	14.32 MPa
$\overline{\Delta Q}$	Max. value within the thickness of the secondary stress range	$M + B$ is 236.61 MPa, $M + B$ is used for Progressive deformation since ratcheting occurs globally across wall. For a Fatigue assessment, total stresses at the local location are to be used. The above reasoning is based on paragraph NH-3213.13 of the ASME B&PVC Section III Subsection NH [11], which distinguishes between General Thermal stress and Local Thermal stress. General Thermal stress is associated with distortion of the structure. Reference [11] gives an example of General Thermal stress that being the equivalent linear stress produced by the radial temperature distribution in a cylindrical shell this being classified as 'Q' while the nonlinear portion of the stress distribution is classified as 'F' for a fatigue assessment. Local thermal stress is associated with almost complete suppression of the differential expansion and so produces no significant distortion. Such stresses shall be considered only from the fatigue standpoint and are therefore classified as peak stresses. Reference [11] gives an example of Local Thermal stress that being the difference between the actual stress and the equivalent linear stress resulting from a radial temperature distribution in a cylindrical shell.
Special case for structures that present secondary membrane stresses:		
Max. $\overline{P_m + Q_m}$	Max. primary plus secondary membrane stress intensity	44.87 MPa to be used for Progressive deformation
Max. $\overline{P_L + P_b + Q_m}$	Max. value of the local primary membrane + primary bending + secondary membrane stress intensity	45.22 MPa to be used for Progressive deformation **Max.** $\overline{P_L + P_b + Q_m}$ is obtained by considering the respective membrane and bending stress components from the finite element analysis stress results, adding these together and then calculating the von Mises stress.

Similarly considering Fig. 9b (Figure RB 3261.1111b [1]) $(\sigma_L + \sigma_b)_N$ is calculated to have a value of 45.218 MPa.

The values for $(\sigma_m)_N$ and $(\sigma_L + \sigma_b)_N$ and Eqs. (1) to 3 are used to determine the required parameters Max(σ_m) and Max($\sigma_L + \sigma_b$) which are shown in Table 8.

Following RB 3261.1114 [1] the secondary ratio in relation to the primary membrane stress SR_1 and the secondary ratio in relation to the sum of primary stresses SR_2 are then calculated. The resulting values of SR_1 and SR_2 given in Table 9.

Following RB 3261.1115 and using the efficiency diagram given in A3.481 [1], the efficiency index v_1 in relation to the primary membrane stress and the efficiency index v_2 in relation to the sum of the primary stresses are calculated and then presented in Table 10. The Efficiency diagram for Eurofer97 steel is not given in RCC-MRx [1] so that use is made of the properties of Group A3.18AS which can be applied for products and parts in alloy steel with approximately 9 % chromium & 1 % molybdenum (X10CrMoVNb9–1) in normalised, tempered or quenched-tempered conditions. Eurofer97 steel has 9 % chromium.

The effective primary stress intensity P_1 is then calculated using RB 3261.1116 [1]

$$P_1 = \frac{Max\ (\sigma_m)}{v_1} = \frac{27.67}{0.2091} = 132.33\ MPa$$

The effective primary stress intensity of the sum of primary stresses P_2 is then given by

$$P_2 = \frac{Max\ (\sigma_L + \sigma_b)}{v_2} = \frac{29.769}{0.2203} = 135.13\ MPa$$

Table 11 compares the values of P_1 and P_2 with the allowables given in RB3261.1117. Both conditions have been satisfied so that progressive deformation will not take place at the stress classification line being considered.

RCC-MRx gives a note that if the secondary stress at the point being analysed results from a temperature transient or from displacement constraints, the value of S_m can be taken to be equal to the mean value of S_m values corresponding to the maximum and minimum values of the mean temperature across the SCL during the period. Here the authors assumed that the secondary stress is cycling from a zero value to maximum and any transient stress excursion is being ignored.

The progressive deformation check was also carried out using the alternative $3S_m$ rule given in (RB 3261.1118). This method is expected to be more conservative and can be used in the absence of creep strains.

The allowable to be satisfied for a period covering all loadings is given by $\text{Max}(\overline{P_L + P_b}) + \overline{\Delta Q} \leq 3S_m$

S_m is the allowable stress calculated previously in Section 2.3 at the maximum value of the mean temperature across the SCL reached during the period of time being considered.

Now

Max$(\overline{P_L + P_b})$ = 14.32 MPa and $\overline{\Delta Q}$ =236.61MPa so that Max$(\overline{P_L + P_b}) + \overline{\Delta Q} = 250.93\ MPa$

Since $3S_m = 3 \times 190.12 = 570.36\ MPa$ then the $3S_m$ criteria is satisfied as well at SCL 10 and progressive deformation will not take place.

2.4.3. The fatigue failure check

The fatigue check is carried out on the SCL under consideration by checking that the fatigue usage fraction $V_A(\overline{\Delta\varepsilon})$ at the SCL is less than unity for all the cycles of loading. For this paper the authors considered only one cycle, the NOC/Dwell cycle for the SCL (referred to as SCL 10) as a means of illustrating the procedure for the fatigue failure check.

For the Fatigue check RB 3261.112 in RCC-MRx [1] is followed. The 'real' strain range $(\overline{\Delta\varepsilon})$ which includes an estimate of the plastic strain (if any) is calculated by using elastic analysis and the cyclic curves given in A3.46. The 'real' strain range $(\overline{\Delta\varepsilon})$ & the fatigue curves A3.47 are then used to calculate the fatigue usage fraction $V_A(\overline{\Delta\varepsilon})$ (RB 3226.2).

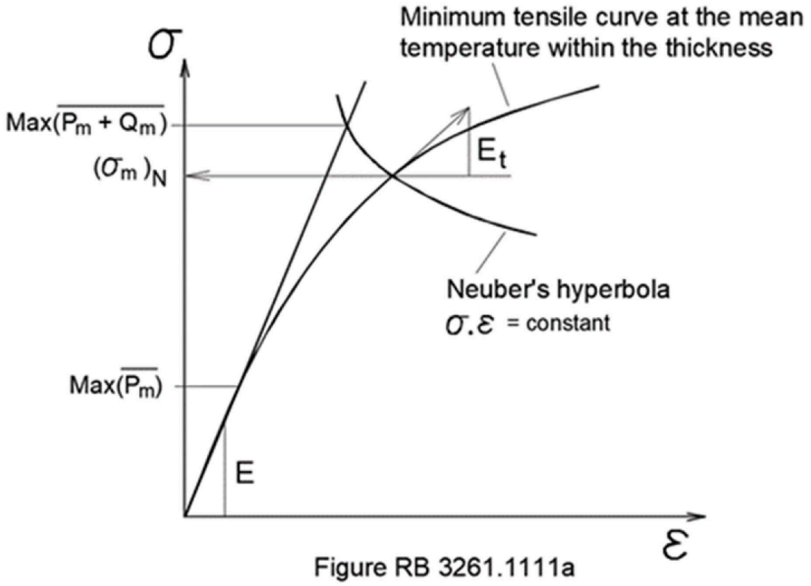

Fig. 9a. Determination of $(\sigma_m)_N$.

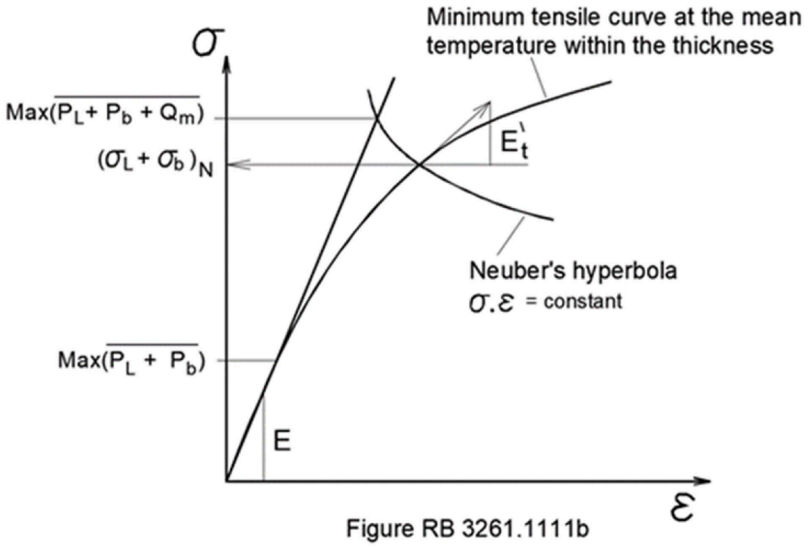

Fig. 9b. Determination of $(\sigma_L + \sigma_b)_N$.

Table 8
Values for the required parameters.

Parameter	Max(σ_m)	Max($\sigma_L + \sigma_b$)	Δq
Value	27.67 MPa	29.769 MPa	236.61 MPa

Table 9
Values for the required parameters (SR_1 & SR_2).

Parameter	SR_1	SR_2
Value	8.551	7.948

Table 10
Values for the required parameters (SR_1 & SR_2).

Parameter	ν_1	ν_2
Value	0.20901	0.2203

Table 11
Comparison of the effective primary stresses with their respective allowables.

Parameter	Allowable	Result
	From A3.18AS.482 [1] $k_{dp1} = k_{dp2} = 1.85$ From Section 2.3, S_m = 190.12 MPa	
$P_1 = 132.33$ MPa	$k_{dp1} \cdot S_m = 351.72$ *MPa*	$P_1 \leq k_{dp1} \cdot S_m$ Satisfied
$P_2 = 135.13$ MPa	$K \cdot k_{dp2} \cdot S_m = 527.58$ *MPa* where RCC-MRx gives K as 1.5 for plates and shells which is the case for the region where there is the stress classification line under consideration	$P_2 \leq K \cdot k_{dp2} \cdot S_m$ Satisfied

The required curves in A3.46 & A3.47 are available for Eurofer97 in the probationary phase rules of RCC-MRx.

The cyclic total stress $\overline{\Delta\sigma}_{tot} = \overline{\Delta(P+Q+F)}$ for the NOC/Dwell cycle can be picked up from Table 4. Extremes of stress intensity and temperatures occur on the inside and outside surface of the cassette so that

the report considers these two points for a fatigue assessment. From Table 4, therefore

$\overline{\Delta\sigma_{tot}}(inside)SCL\ 10 = 300.93\ MPa\ (\text{Max. } \theta = 230.44^oC)$

$\overline{\Delta\sigma_{tot}}(outside)SCL\ 10 = 162.52\ MPa\ (\text{Max. } \theta = 347.84^oC)$

The cyclic strain to be used in the fatigue curves is given by $\overline{\boldsymbol{\Delta\varepsilon}}$ equal to the sum of the four terms $\overline{\Delta\varepsilon_1}$, $\overline{\Delta\varepsilon_2}$, $\overline{\Delta\varepsilon_3}$, $\overline{\Delta\varepsilon_4}$.

The above four strain terms are determined using the cyclic curves (A3.46) corresponding to the highest temperature (Max. $\theta = 230.44^oC$) and (Max. $\theta = 347.84^oC$) at the inside and outside surface of the cassette at SCL 10.

The material properties required for a fatigue assessment are those determined at the local temperature of the point under consideration. This is so because fatigue is a local type of failure rather than a global type.

For Eurofer97 $R_{p0.2\ min}$ is given in A3.41 as a function of temperature and the calculated values at the required temperatures are shown in Table 12.

Since $R_{p0.2\ min}$ at the local temperature is larger than $\overline{\Delta\sigma_{tot}}(inside) = 300.93\ MPa$ and $\overline{\Delta\sigma_{tot}}(outside) = 162.52\ MPa$ then it is expected that the 'plastic' increase in strains $\overline{\Delta\varepsilon_2}$ & $\overline{\Delta\varepsilon_3}$ will have a value of zero or at least be very small. This statement is valid for this particular situation in which most stress comes from the thermal loading which is cycling. In other cases, the statement may not be correct since there may be a high level of constant stress but low cyclic stresses.

Calculating the elastic strain range $\overline{\Delta\varepsilon_1}$

To calculate the elastic strain range $\overline{\Delta\varepsilon_1}$ use is made of Diagram 1 of the RCC-MRx Figure RB 3261.1123 here shown in Fig. 10. This essentially says that $\overline{\Delta\varepsilon_1}$ is the elastic strain range calculated at $\overline{\Delta\sigma_{tot}}$.

Following RCC-MRx use must be made of the formula $\overline{\Delta\varepsilon_1} = \frac{2}{3}(1+\nu).\left(\frac{\overline{\Delta\sigma_{tot}}}{E}\right)$ where E is the Young's modulus at temperature Max θ (A3.22) and ν is the Poisson's ratio (A3.23). The equation for $\overline{\Delta\varepsilon_1}$ is consistent with the cyclic half life curve A3.19AS.461 used to determine $\overline{\Delta\varepsilon_2}$ and $\overline{\Delta\varepsilon_3}$.

The Young's Modulus, E, for Max θ = 230.44 °C and for Eurofer steel is calculated to be 205,687 MPa.

For elastic analyses the Poisson's ratio ν is taken as 0.3.

Therefore at the inside surface $\overline{\Delta\varepsilon_1} = \frac{2}{3}(1 + 0.3).\left(\frac{300.93}{205687}\right) = 0.126798\%$

Similarly $\overline{\Delta\varepsilon_1}$ at the outside surface of SCL 10 given by $\overline{\Delta\varepsilon_1} = 0.07067\%$

Calculating the strain range $\overline{\Delta\varepsilon_2}$

$\overline{\Delta\varepsilon_2}$ represents the 'plastic' increase in strain due to the primary stress range at the point under examination. RCC-MRx says that the value of $\overline{\Delta\varepsilon_2}$ is generally very low but care needs to be taken if there is appreciable elastic follow-up. The amount of elastic follow-up can be determined by calculating the follow up factor 'r'. An explanation of the latter is given in the companion paper Part I – General Discussion [12].

Diagram 2 of RCC-MRx Figure RB 3261.1123 here shown in Fig. 11 and the cyclic curves A3.46 are used to calculate $\overline{\Delta\varepsilon_2}$.

The primary stress range is equal to $\overline{\Delta(P_m + 0.67(P_b + P_L - P_m))}$

In this case, for the NOC/Dwell cycle the primary stress range is equal to zero since it is only the secondary stress that is cycling.

Table 12
The values of $R_{p0.2\ min}$ at the required temperatures for the fatigue assessment (A3.41).

Temperature, θ	$R_{p0.2\ min}$
230.44^oC	447.86 MPa at the inside surface at SCL 10
347.84^oC	420.57 MPa at the outside surface at SCL 10

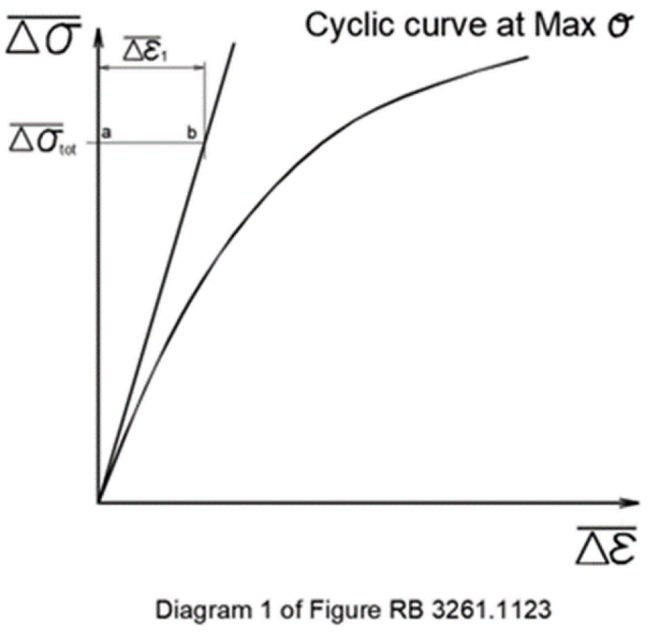

Fig. 10. Diagram 1 of RCC MRx Figure RB 3261.1123 used to calculate $\overline{\Delta\varepsilon_1}$.

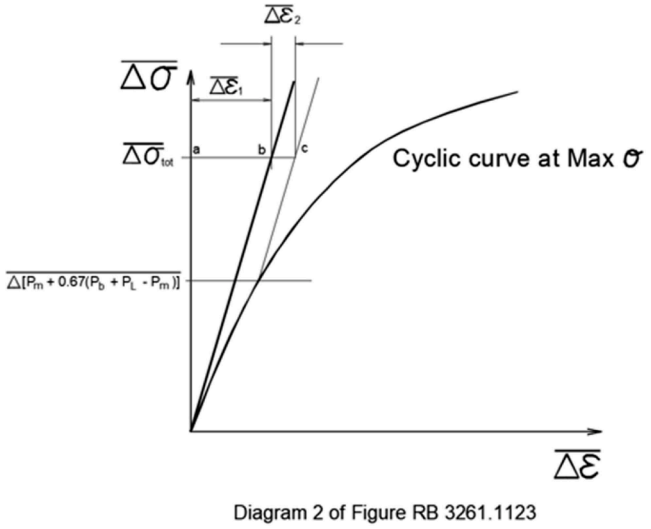

Fig. 11. Diagram 2 of RCC MRx Figure RB 3261.1123 used to calculate $\overline{\Delta\varepsilon_2}$.

Therefore for both the inside and outside surfaces for SCL 10 $\overline{\Delta\varepsilon_2} = 0\%$

Calculating the strain range $\overline{\Delta\varepsilon_3}$

$\overline{\Delta\varepsilon_3}$ represents the 'plastic' increase in strain along path (cd) of Diagram 3 of RCC-MRx Figure RB 3261.1123 here shown in Fig. 12. Point (d) is the intersection point of the cyclic curve and Neuber's hyperbola passing through point (c).

For the inside surface point 'c' or in this case Point 'b' since $\overline{\Delta\varepsilon_2} = 0$ % has coordinates 300.93 MPa and 0.12679 % so that Neuber's hyperbola is given by

$\overline{\Delta\sigma}.\overline{\Delta\varepsilon} = 300.93 \times 0.126798 = 38.1572$

The half life cyclic curve is given by the formula as $\overline{\Delta\varepsilon_t}\ (\%) = 100.\frac{2(1+\nu)}{3E}(\overline{\Delta\sigma}) + \left(\frac{\overline{\Delta\sigma}}{K}\right)^{\frac{1}{m}}$ where E is the Young's modulus function at temperature = 205,687 MPa (calculated previously)

K, m are coefficients from Table A3.19AS.461[1] which for θ = 230.44 °C are given by $K = 764$ MPa and $m = 0.1185$ so that the half

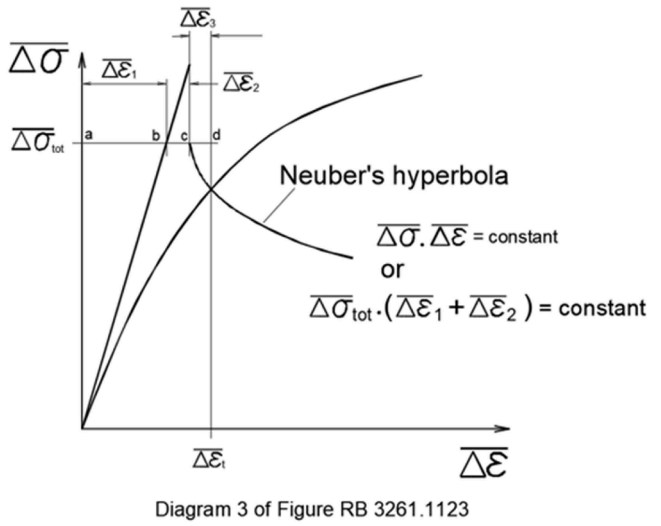

Fig. 12. Diagram 3 of RCC MRx Figure RB 3261.1123 used to calculate $\overline{\Delta\varepsilon_3}$.

life cyclic curve is given by

Therefore $\overline{\Delta\varepsilon_t}$ (%) $= 4.214 \times 10^{-4}(\overline{\Delta\sigma}) + \left(\frac{\overline{\Delta\sigma}}{764}\right)^{8.4388}$

From Neuber's hyperbola $\overline{\Delta\varepsilon} = \frac{38.1572}{\overline{\Delta\sigma}}$

The intersection point of the two functions results in a value of $\overline{\Delta\sigma} = 300.463$ MPa and corresponding $\overline{\Delta\varepsilon} = 0.12699$%.

Therefore $\overline{\Delta\varepsilon_3} = \overline{\Delta\varepsilon} - \overline{\Delta\varepsilon_1} - \overline{\Delta\varepsilon_2} = 0.12679 - 0.12699 - 0 = -0.0002\ \% = 0\ \%$

The negative sign is deemed due to numerical errors and shows that there is no plasticity occurring on the inside surface at SCL 10. This as predicted previously.

For the outside surface similar calculations are carried out so that once again $\overline{\Delta\varepsilon_3}$ is calculated to be equal to zero showing that there is no plasticity occurring on the outside surface at SCL 10.

Calculating the strain range $\overline{\Delta\varepsilon_4}$

$\overline{\Delta\varepsilon_4}$ is defined in RCC-MRx RB 3261.1123 as the 'plastic' increase in strain due to triaxiality. For cases of perfect biaxiality such as for the case of the skin surface under thermal shock $\overline{\Delta\varepsilon_4} = (K_v - 1)\ .\ \overline{\Delta\varepsilon_1}$

K_v is called the amplification coefficient and is evaluated using the Curves and/or the Tables in A3.463 for temperature Max θ.

For the inside surface at SCL 10, $\Delta\varepsilon_1 = 0.1268$%, $\overline{\Delta\sigma_{tot}} = 300.93\ MPa$ and $\theta = 230.44$ °C so that using the RCC-MRx Table A3.19AS.463, K_v=1.001

Therefore $\overline{\Delta\varepsilon_4} = (K_v - 1)\ .\ \overline{\Delta\varepsilon_1} = (1.001 - 1).\ 0.1268\% = 0.0001268\ \%$

Similarly for the outside surface for SCL 10 $\overline{\Delta\varepsilon_4}$ was calculated to have a value of 0 %

For other cases other than perfect biaxiality RCC MRx remarks that the calculation of $\overline{\Delta\varepsilon_4}$ as given above is excessive so that K_v may be reduced by multiplying it by the coefficient $\sqrt{\frac{\left[1+3\left(\gamma^2/K_v^2\right)\right]}{(1+3\gamma^2)}}$ where $\gamma = \frac{\Delta\sigma_1 - \Delta\sigma_2}{\Delta\sigma_1 + \Delta\sigma_2}$ and $\Delta\sigma_1$ and $\Delta\sigma_2$ are the elastic stress ranges in the two principal directions.

The values of $\overline{\Delta\varepsilon_4}$ for SCL 10 are small (one of them actually having a value of zero) so that the authors decided that there is no need to reduce K_v for this stress classification line. In case of relative high values for $\overline{\Delta\varepsilon_4}$ the authors recommend to analyse the biaxiality or triaxiality of the stress field at the point under consideration so that if possible the value of K_v is reduced. This would result in a higher predicted fatigue life. Having said that, if this reduction is not taken into consideration, then the fatigue life calculated is conservative.

The 'real' strain range $(\overline{\Delta\varepsilon})$ *and calculating the fatigue lives*

For the inside surface at SCL 10:

$\overline{\Delta\varepsilon} = \overline{\Delta\varepsilon_1} + \overline{\Delta\varepsilon_2} + \overline{\Delta\varepsilon_3} + \overline{\Delta\varepsilon_4} = 0.1429 + 0 + 0 + 0.0001268 = 0.143\ \%$

For the outside surface for SCL 10:

$\overline{\Delta\varepsilon} = \overline{\Delta\varepsilon_1} + \overline{\Delta\varepsilon_2} + \overline{\Delta\varepsilon_3} + \overline{\Delta\varepsilon_4} = 0.0792 + 0 + 0 + 0 = 0.0792\ \%$

By using the fatigue curves in RCC-MRx A3.47 at the respective temperature and cyclic strain shown in Table 13, the fatigue lives at the inside and outside surfaces at SCL 10 were calculated to be larger than 1 million cycles

2.5. Comparison of results for SCL 10 in the divertor cassette

Fig. 8 shows the postprocessing script results for SCL 10 of the Divertor cassette and as presented in [2]. For the Type P and Type S ratchetting checks the numbers under the column 'NOC' give the allowable stress divided by the calculated value of the relevant stress from the cassette model. This means that a number larger than unity shows that the SCL has passed that particular check. For Type S Fatigue usage, a number larger than 100 % means that the Fatigue check has failed. Table 14 shows the comparison of results between the authors` work and those presented in [2]. For the Type P checks and for the Type S effective primary membrane stress intensity check the results match quite well. On the other hand for the Type S effective primary membrane plus bending stress intensity check and the fatigue check the results are not in agreement. For the Fatigue assessment the result obtained in this paper does not predict failure due to fatigue as opposed to the result in [2].

Disagreements in the results comparison may have occurred due to either different code interpretations or due to programming/algorithm errors in the post processing script. This highlights the importance of correct code interpretations between different stress analysts. In addition, using a verified post processing script to analyse finite element results according to the design code is also particularly important. The post processing script captures correct code interpretation that can be verified in-house by a number of stress analysts. This results in use of best practice and at the same time reduces human errors while working through the code rules and procedures.

3. Structural integrity assessment for the SCL results in the region of high stress where the temperature is above the creep threshold

This section concentrates on the NOC load case at a stress classification line in the region of high stress and at which the temperature is above the creep threshold. This SCL is in the shielding liner of the divertor. The elastic design by analysis rules of RCC-MRx [1] were followed and comparison was also made with results obtained in [3] which used the finite element analysis postprocessing script that was developed in house and based on the RCC-MRx code rules.

In contrast with the previous section, the detailed calculations performed for the structural integrity check at the concerned SCL will not be shown here. Instead, after an introduction, some results for the Type P and Type S checks are given and observations made by the authors while following the RCC MRx design rules applied to this particular SCL are highlighted. Some discussions and conclusions are then also given

Table 13
Data used to determine the fatigue lives at the inside and outside surfaces of SCL 10.

Location	$\overline{\Delta\varepsilon}$	θ
Inside surface SCL 10	0.143 %	230.44 °C
Outside surface SCL 10	0.0792 %	347.84 °C

Table 14
Comparison of results between the authors' work and those presented in [2].

Failure mode	Current results	Percentage difference from Reference [2] (Fig. 11)
Type P		
$\overline{P_m}, \overline{P_L}$	$\frac{190.12}{10.47} = 18.16$	0 %
$\overline{P_L + P_b}$	$\frac{190.12 \times 1.5}{14.32} = 19.91$	0.9 %
Type S Progressive deformation		
Effective primary membrane stress intensity	$\frac{351.72}{132.33} = 2.66$	0 %
Effective primary membrane + bending stress intensity	$\frac{527.58}{135.13} = 3.9$	37.4 %
Type S Fatigue		
	Does not predict failure	Predicts failure

including comparison with results obtained in [3].

Fig. 13 shows the position and orientation of the SCL in the Shielding liner in the region of high stress. The temperature along the path is shown in Fig. 14, There is no stress singularity at the SCL and for load cases 1, 2, 3, 4, the temperature is above the creep threshold of 375 °C up to one-third-the length of the path from the outer surface of the shielding liner.

Figs. 15a and 15b show the von Mises stress plots near the region of the SCL for load case 1 which is the thermal load case and for load case 2 which is the NOC load case respectively. The plots confirm that the stress classification line is not in a stress singularity region although the change in geometry at the cooling channel creates some stress concentration.

The stress classification line under consideration is referred to as SCL 3 in [3].

3.1. Primary, secondary and total stresses

3.1.1. Table of linearised stresses, total and cyclic stresses for SCL 3 (shielding liner) and load case NOC

Table 15 shows the linearised, total and cyclic stresses at SCL 3 used in the RCC MRx assessment for load case 2 which is the NOC load case. For membrane plus bending and for total stresses, both values on the inside and outside surfaces along SCL 3 are being shown. Similarly details such as temperature and temperature ranges at the point are also shown. The stress categories shown in column 1 are as those defined by RCC-MRx [1] and all the stress values are obtained from the finite element model for the shielding liner of the divertor. The secondary cyclic stress values for the NOC/Dwell cycle are also shown.

In this paper the secondary stress is that obtained from the application of the thermal load alone in load case 1. The NOC load case includes the thermal load, 3.5 MPa cooling water pressure, the ferromagnetic load and the effect of gravity.

The primary stress through thickness for SCL 3 for load case 2 (NOC) was obtained by using load combinations in ANSYS Mechanical [8] by subtracting the thermal secondary stress field (load case 1) from the Primary + Secondary stress field [3].

As can be seen in Table 15, contrary to what one would expect, most of the times, the total stress on the outside surface of the shielding liner, is lower than the membrane plus bending stress. This also happens at stress component level. The same situation was encountered in Section 2 for SCL 10 in the divertor cassette and may require assessment using an elastic plastic approach in order to check on the validity of the elastic approach to DBA for such components.

The mean wall temperature θ_m was calculated to be 348 °C. This is below the creep strain threshold for Eurofer97 steel. At this temperature, the 0.2 % proof stress $R_{p\ 0.2\ min.}$ is equal to 420 *MPa*. At the outside wall temperature of 399.67°C the 0.2 % proof stress $R_{p\ 0.2\ min.}$ is equal to 401 MPa.

3.1.2. Summary of results from reference [3] for SCL3

Table 16 shows the results for SCL 3 as obtained from [3]. The latter used the in-house developed finite element post processing script for the analysis. The purpose of the next sections is to give results from a structural integrity assessment for SCL 3 (Shielding Liner) following RCC-MRx and performed by the authors and then compare the results with those shown in Table 16 for the NOC Load case. Difficulties and issues encountered in code interpretation and implementation to perform the assessment of the DEMO divertor cassette are further discussed.

3.2. Creep, irradiation and ageing checks

3.2.1. The negligible creep test - RB 3216.1

For load steps 1, 2, 3, 4, the temperature is above 375 °C up to one-third-the length of SCL 3 from the outer surface of the shielding liner (Fig. 14). The temperature varies from 236.2 °C on the inside surface to 399.67 °C on the outside surface of the shielding liner. For Eurofer97 steel the temperature threshold for creep is 375 °C whatever the holding time (RCC-MRx A3.31) so that strains due to creep are accepted to take place through part of the wall thickness. Having said this, the Type P checks for plastic instability and excessive deformation and the Type S check for progressive deformation are associated with global failure or excessive deformation over the entire structural wall thickness. This means that the mean wall temperature of 348 °C is used for determining the material properties for the latter checks. The mean wall temperature is below the Eurofer97 threshold for creep so that creep is not considered for the Type P checks for plastic instability and excessive deformation and the Type S check for progressive deformation.

In RB 3261.1118 gives the alternative $3S_m$ rule which is only valid

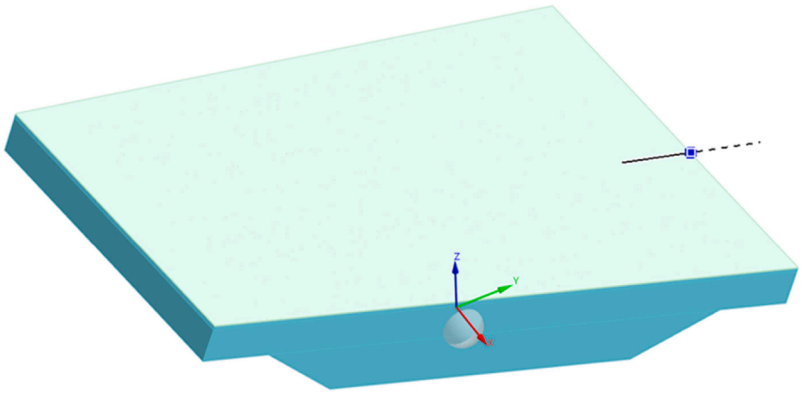

Fig. 13. Position and orientation of the coordinate system of the SCL under consideration in the shielding liner (finite element view).

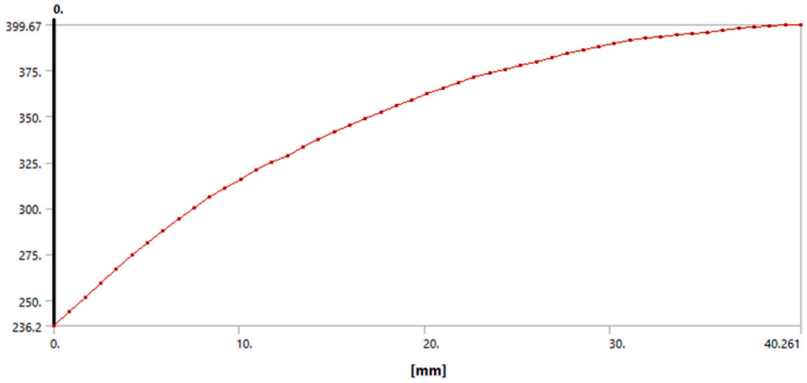

Fig. 14. Temperature distribution across the SCL under consideration in the shielding liner (Load cases 1 to 4).

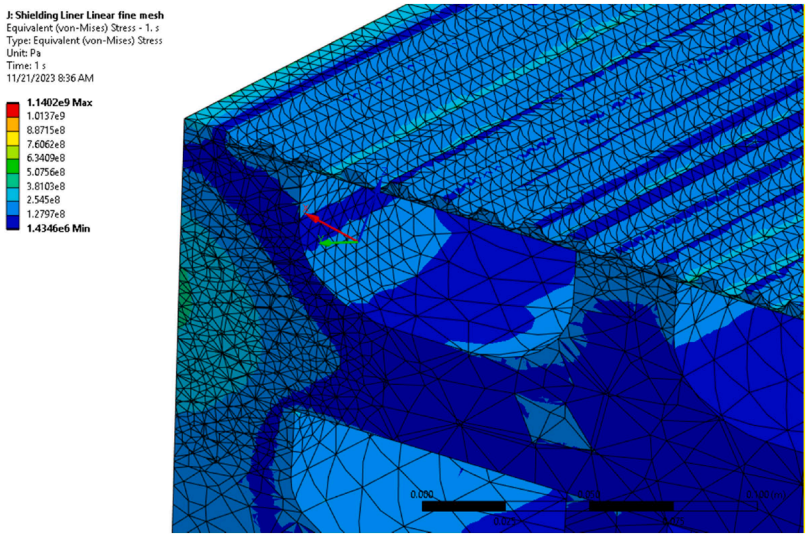

Fig. 15a. Load case 1: Secondary stress (Thermal load) for NOC, EM & SL 1 loading.

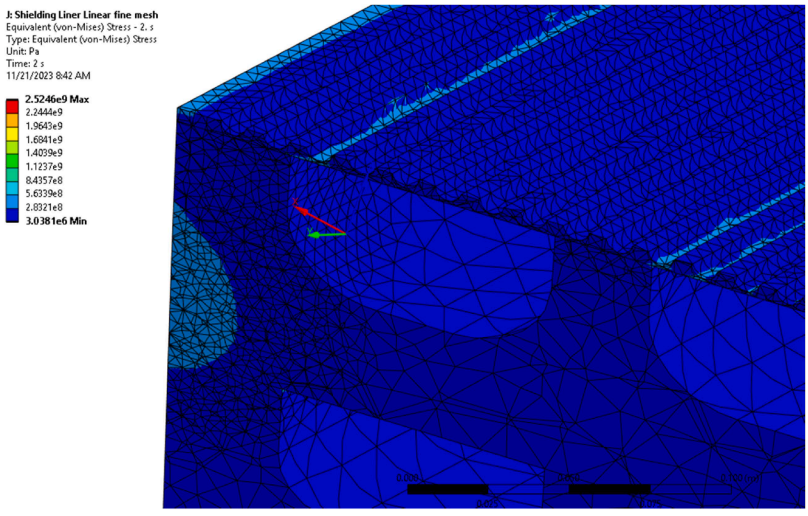

Fig. 15b. Load case 2: NOC (includes Thermal load, 3.5 MPa pressure, Ferromagnetic & Gravity).

for cases where the temperature is below the creep threshold. RCC MRx requires the check to be made at all points of the structure so that the $3S_m$ rule is not valid for the end of SCL3 lying on the outer surface of the shielding liner.

The fatigue check, is associated with local type of failure so that such a check performed on the outside wall at SCL 3 where the temperature is above the creep threshold must use significant creep rules. This would entail a creep fatigue assessment at this point.

Table 15
Linearised stresses for SCL 3 used in the structural integrity assessment (Load case NOC).

Type of stress category	Temperature °C	Membrane MPa	Membrane ± Bending MPa		Total MPa	
Secondary	T_{inside} =236.2	190.56	48	391	144	373
NOC	$T_{outside}$ = 399.67		(Inside)	(Outside)	(Inside)	(Outside)
Primary ± Secondary	T_{inside} =236.2	193.47	50.67	392.49.56	158.44	373
NOC	$T_{outside}$ = 399.67		(Inside)	(Outside)	(Inside)	(Outside)
Primary	T_{inside} =236.2	15.2	24.23	10.12	28.99	10.55
NOC	$T_{outside}$ = 399.67		(Inside)	(Outside)	(Inside)	(Outside)
$\overline{\Delta Q}$ NOC/Dwell	ΔT_{inside} = (236.2 −180)	171.39	65.73	356.87	228.98	322.16
	$\Delta T_{outside}$ = (399.67 −180)		(Inside)	(Outside)	(Inside)	(Outside)

Table 16
Summary of results for SCL 3 from reference [3] (NOC load case).

Creep check	TRUE
Type P Assessment	TRUE
Type P Membrane	12.07
Type P Membrane + Bending	10.64
Type P Creep	0.46
Type S Assessment	FALSE
Type S Ratcheting Membrane	1.25
Type S Ratcheting Membrane + Bending	1.52
Type S Fatigue usage	9.67
Type S Ratcheting Membrane Creep	2.65E-06
Type S Ratcheting Membrane + Bending Creep	4.768E-08

3.2.2. Irradiation & aging tests - RB 3216.2 & RB 3216.3

Irradiation and aging have not been considered so that rules for negligible irradiation RB 3251.1 for Type P damage and RB 3261.111 to RB 3261.113 for Type S damage Progressive Deformation and Fatigue, respectively are followed.

3.3. Preventing type P damages - negligible creep & negligible irradiation - RB 3251.1 – level A criteria

Table 17 shows the numerical data required for the Type P check and obtained from Table 15. Table 18 shows the comparison of stresses with their respective allowables for the Type P check. In Table 18, $S_m(\theta_m)$ is the allowable stress given in A3.43 [1] at the mean temp. θ_m (348 °C) calculated along the SCL.

The conclusion from Table 18 is that all the allowable stresses for the Type P check are satisfied for the stress classification line under consideration (SCL 3).

3.4. Preventing type S damages – cycle considered is NOC / dwell

3.4.1. The normal operation NOC / dwell cycle

During the NOC load case the loads being applied are the thermal map load, the cooling water pressure, the ferromagnetic, and earth gravity.

During the Dwell load case the loads being applied are the thermal load at 180 °C uniform temperature, the cooling water pressure, the ferromagnetic and earth gravity.

Therefore, the cyclic load is the secondary one and is due to thermal cycling between the NOC temperature distribution and the Dwell 180 °C uniform temperature distribution. Table 19 gives the required values for the primary membrane, the primary membrane plus bending stresses and the cyclic stress range for SCL 3 in the shielding liner.

Table 17
Numerical Data required for the Type P check.

Parameters:	Definition:	Value: (From Table 15)
$\overline{P_m}$	General primary membrane stress intensity	15.2 MPa
$\overline{P_L}$	Local primary membrane stress intensity	15.2 MPa (No discontinuity)
$\overline{P_L + P_b}$	Primary membrane plus bending stress intensity	24.23 MPa

Table 18
Comparison of stresses for the Type P check.

Stress allowables:	Notes:	S_m=183.36 MPa
$\overline{P_m} \le S_m(\theta_m)$	SCL 3 far away from a local or geometric discontinuity	$\overline{P_m}$ = 15.2 MPa < S_m Allowable is satisfied
$\overline{P_L} \le 1.5 S_m(\theta_m)$	SCL 3 far away from a local or geometric discontinuity so that $\overline{P_L} = \overline{P_m}$	$\overline{P_L}$ = 15.2 MPa < 1.5S_m Allowable is satisfied
$\overline{P_L + P_b} \le 1.5 S_m(\theta_m)$	SCL 3 far away from a local or geometric discontinuity	$\overline{P_L + P_b}$ = 24.23 MPa < 1.5S_m Allowable is satisfied

For the progressive deformation check the maximum mean temperature over the cycle is used in order to calculate the required material properties. This is because progressive deformation failure is related to the global ratchetting failure of the structural wall. On the other hand, the fatigue check requires the local temperature to be used for calculating the required material properties since fatigue failure is a local type of failure. Membrane plus bending ($M + B$) and total stresses are used for the progressive deformation check and for the fatigue check respectively for the same reasons.

Table 15 for the NOC secondary stress category shows that there is a secondary membrane stress of 190.56 MPa so that the RCC-MRx progressive deformation check rules followed are those associated with the 'Special case for structures that present secondary membrane stress'. It must be also noted that to calculate Max. $\overline{P_L + P_b} + \overline{Q_m}$ the addition between $\overline{P_L + P_b}$ and $\overline{Q_m}$ must be carried out at stress tensor component level and the von Mises stress is then calculated.

3.4.2. The progressive deformation failure check

Similar calculations to the ones shown in Section 2.4.1 are carried out to determine the effective primary stress intensity P_1 = 469.58 MPa and the effective primary stress intensity of the sum of primary stresses P_2 = 256.24 MPa.

Table 20 compares the values of P_1 and P_2 with the allowables given in RB3261.1117. The allowable for P_2 was satisfied but this is not so for P_1. Since the allowable for P_1 was not satisfied there is a risk that Progressive Deformation will take place at SCL 3 of the shielding liner.

Given that the mean wall temperature is below the creep threshold temperature and that progressive deformation is considered to occur globally rather than locally, the latter check was also carried out by using the alternative 3S_m rule given in (RB 3261.1118).

The allowable to be satisfied for a period covering all loadings is given by Max$(\overline{P_L + P_b})$ + $\overline{\Delta Q}$ $\le 3S_m$

S_m is the allowable stress calculated previously at the maximum

Table 19
Numerical data used for the Progressive deformation and Fatigue checks.

Parameters:	Definition:	Value: (From Table 4)
Max. θ_m	Max. value of the mean temp. through the thickness	348 °C
Max. $\overline{P_m}$	Max. value of the primary membrane stress intensity	15.2 MPa
Max. $\overline{P_L + P_b}$	Max. value of the primary membrane plus primary bending stress intensity	24.23 MPa
$\overline{\Delta Q}$	Max. value within the thickness of the secondary stress range	$M+B$ is 356.87 MPa, $M+B$ is used for Progressive deformation since ratcheting occurs globally across wall. For a Fatigue assessment, total stresses at the local location are to be used. The above reasoning is based on paragraph NH-3213.13 of the ASME B&PVC Section III Subsection NH [11], which distinguishes between General Thermal stress and Local Thermal stress. General Thermal stress is associated with distortion of the structure. Reference [11] gives an example of General Thermal stress that being the equivalent linear stress produced by the radial temperature distribution in a cylindrical shell this being classified as 'Q' while the nonlinear portion of the stress distribution is classified as 'F' for a fatigue assessment. Local thermal stress is associated with almost complete suppression of the differential expansion and so produces no significant distortion. Such stresses shall be considered only from the fatigue standpoint and are therefore classified as peak stresses. Reference [11] gives an example of Local Thermal stress that being the difference between the actual stress and the equivalent linear stress resulting from a radial temperature distribution in a cylindrical shell.
Special case for structures that present secondary membrane stresses:		
Max. $\overline{P_m + Q_m}$	Max. primary plus secondary membrane stress intensity	193.47 MPA to be used for Progressive deformation
Max. $\overline{P_L + P_b + Q_m}$	Max. value of the local primary membrane + primary bending + secondary membrane stress intensity	195 MPa to be used for Progressive deformation **Max.** $\overline{P_L + P_b + Q_m}$ **is** obtained by considering the respective membrane and bending stress components from the finite element analysis stress results.

Table 20
Comparison of the effective primary stresses with their respective allowables.

Parameter	Allowable	Result
	From A3.18AS.482 [1] $k_{dp1} = k_{dp2} = 1.85$ From Section 3.3, S_m = 183.36 MPa	
$P_1 = 469.58$ MPa	$k_{dp1} \cdot S_m = 339.22$ *MPa*	$P_1 \leq k_{dp1} \cdot S_m$ Not Satisfied
$P_2 = 256.24$ MPa	$K \cdot k_{dp2} \cdot S_m = 508.82$ *MPa* where RCC-MRx gives K as 1.5 for plates and shells which is the case for the region where there is the stress classification line under consideration	$P_2 \leq K \cdot k_{dp2} \cdot S_m$ Satisfied

value of the mean temperature across the SCL reached during the period of time being considered.

Now, for the inside wall surface

$\text{Max}(\overline{P_L + P_b})$ = 24.23 MPa and $\overline{\Delta Q}$ = 65.73MPa so that $\text{Max}(\overline{P_L + P_b}) + \overline{\Delta Q} = 89.96$ *MPa*

For the outside wall surface

$\text{Max}(\overline{P_L + P_b})$ = 10.12 MPa and $\overline{\Delta Q}$ = 356.87MPa so that $\text{Max}(\overline{P_L + P_b}) + \overline{\Delta Q} = 367$ *MPa*

Since $3S_m = 3 \times 183.36 = 550.08$ *MPa* then the $3S_m$ criteria is satisfied at SCL 3 in the shielding liner both on the inside surface and on the outside surface so that according to this criterion progressive deformation will not take place. Having said this, the authors wish to make a comment that the $3S_m$ rule is not valid for the end of SCL3 lying on the outer surface of the shielding liner because the temperature is higher than the creep threshold temperature. This means that the latter conclusion is not valid.

In contrast to the results shown in Table 20, the in-house developed finite element post processing script does not predict progressive deformation at SCL 3 so that the above issue needs some more investigation.

Given the mismatch of the result obtained in this paper and that from the in-house postprocessing script the authors decided to perform a further investigation by considering the case of no secondary membrane stress within the RCC-MRx rules rather than a case of secondary membrane stress (Q_m is non zero in the stress linearisation output).

Table 21 shows the values for P_1 and P_2 calculated when considering the case of no secondary membrane stress. Table 21 indicates that the allowables for P_1 and P_2 are both satisfied when considering the case when there is no secondary membrane stress. This means that, for this case, progressive deformation is not predicted at SCL 3 of the shielding liner agreeing with the result obtained using the in-house finite element post processing script and with the $3S_m$ rule. The latter does not agree with the result presented previously when the case of secondary membrane stress is considered.

These conflicting results for the progressive failure check require further investigation into the use of the RCC-MRx rules applied to the structural integrity assessment of the DEMO divertor components.

3.4.3. The fatigue failure check

Section 3.4.1 concludes with some conflicting results on the progressive failure check. When considering the case of secondary membrane stress and using the effective primary stress method the authors concluded that progressive deformation will take place at SCL 3. RCC-MRx requires that progressive deformation does not occur in order to be able to use the rules to prevent fatigue damage. Given the conflicting

Table 21
Comparison of the effective primary stresses with their respective allowables (case of no secondary membrane stress).

		Allowables:
$P_1 = 150.5$ MPa	$k_{dp1} \cdot S_m = 339.2$ *MPa*	$P_1 \leq k_{dp1} \cdot S_m$ Satisfied
$P_2 = 171.36$ MPa	$K \cdot k_{dp2} \cdot S_m = 508.8$ *MPa*	$P_2 \leq K \cdot k_{dp2} \cdot S_m$ Satisfied

results and the failure of the negligible creep progressive deformation check, no further Type S analysis, i.e. that of significant creep and creep fatigue, were carried out on SCL 3 of the shielding liner.

3.5. Comparison of results for SCL 3

Table 16 shows the finite element analyses postprocessing script results for SCL 3 of the shielding liner and as presented in [3]. For the Type P and Type S progressive deformation checks the numbers under the column 'NOC' give the allowable stress divided by the calculated value of the relevant stress from the shielding liner model. This means that a number larger than unity shows that the SCL has passed that particular check. For Type S Fatigue usage, a number larger than 100 % means that the Fatigue check has failed.

Table 22 shows the comparison of results between the authors` work and that presented in [3]. For the Type P membrane check the result matches quite well. For the Type P membrane plus bending check there is a difference of 6.3 %. The percentage difference increases to 44.4 % and 48.8 % for the Type S Progressve deformation checks when considering the effective primary membrane stress intensity and the effective membrane plus bending stress intensity and the case of no secondary membrane stress. When the secondary membrane stress is taken into consideration the authors predict failure for the Type S Progressve deformation checks when considering the effective primary membrane stress intensity. This is not so from the results presented in [3]. For the case of secondary membrane stress and considering the Type S progressive deformation checks and the Effective primary membrane + bending stress intensity the percentage difference is 23.6 %.

In this paper, a fatigue assessment is not presented since it was predicted that the progressive deformation check failed. In contrast, reference [3] does not predict failure due to fatigue.

Disagreements in the results comparison may have occurred due to either different code interpretations or due to programming/algorithm errors in the post processing script. This highlights the importance of correct code interpretations between different stress analysts. In addition, using a verified post processing script to analyse finite element results according to the design code is also particularly important.

Using a verified post processing script to analyse finite element results according to the design code is also particularly important. The post processing script should capture correct code interpretation that can be verified in-house by a number of stress analysts. This results in use of best practice and at the same time reduces human errors while working through the code rules and procedures.

Table 22
Comparison of results between the authors' work and those presented in [3].

Failure mode	Current results	Percentage difference from Reference [3] (Table 16)
Type P		
$\overline{P_m}$, $\overline{P_L}$	$\frac{183.36}{15.2} = 12.06$	0.08 %
$\overline{P_L + P_b}$	$\frac{183.36 \times 1.5}{24.23} = 11.35$	6.3 %
Type S Progressive deformation		
Effective primary membrane stress intensity	$\frac{339.2}{469.58} = 0.72$ (Case of secondary membrane stress) $\frac{339.2}{150.5} = 2.25$ (Case of no secondary membrane stress)	Allowable not satisfied, no percentage difference comparison is shown 44.4 %
Effective primary membrane + bending stress intensity	$\frac{508.8}{256.24} = 1.99$ (Case of secondary membrane stress) $\frac{508.8}{171.36} = 2.97$ (Case of no secondary membrane stress)	23.6 % 48.8 %
Type S Fatigue		
	Fatigue check not done since progressive deformation check fails	Reference [3] predicts failure

4. Discussion and conclusions

Most structural integrity analysts agree that the elastic approach to Design by Analysis (DBA) is quite subjective at times so that its usefulness highly depends on the skill and experience of the analyst. Special care must be taken from the side of the analyst as where to locate SCLs in order to capture the possibility of different failure modes.

For box type of structures the codes do not give much guidance for performing stress classification, especially in regions of stress concentration. For example, in such regions, the analyst is required to differentiate between local primary membrane stress and general primary membrane stress. Different allowable stresses are applied to these different stress categories. The code rules for such type of structures may be interpreted differently by different stress analysts so that more guidelines for best practice must be further developed for consistent analysis.

This paper considers the elastic DBA approach of RCC MRx and highlights some queries, difficulties and issues of interpretation encountered when performing DBA calculations on two stress classification lines: one in the Divertor cassette and one in the Shielding liner of the cassette. Comparison is made with results obtained using a finite element analysis post processing script developed independently within the EUROfusion DEMO divertor design group and following elastic DBA.

Difficulties of code implementation when using RCC MRx code rules arise in areas where there are stress singularities and where data, such as material data in the irradiated state for Eurofer97 steel, is limited. The divertor cassette is above the negligible irradiation level and so this raises serious concerns in being able to perform design checks under irradiated conditions. The current dual circuit model of the DEMO divertor has a number of mathematical stress singularities referred to as geometrical discontinuities in RCC MRx at which it is not possible to determine the stress value. This means that checks that require the total stress at a stress singularity are not possible unless a method is developed to deal with such stress singularities.

Currently, RCC MRx only gives the creep threshold temperature for Eurofer97 steel. The code does not provide the latter material negligible creep curve. This limits the negligible creep tests that need to be carried out in order to exclude or include the creep rules over the entire lifetime of the component. Not having the negligible creep curve and having to consider creep, when the negligible creep temperature is exceeded, makes the assessment more conservative because the significant creep rules must be followed. The lowest temperature at which the material properties for creep rupture stress are available is 425 °C and the latter has to be used for the assessment in case that significant creep rules have to be followed even if the temperature for the region under consideration is at a temperature below 425 °C but above the creep threshold.

The paper also highlights the importance of the phenomenon of elastic follow up which needs to be addressed in order to differentiate between secondary and primary stresses developed from loads that at face value create secondary stresses. For such cases the paper suggests literature that provide methods to determine the elastic follow up factor. This factor is important for the stress analyst when it comes to stress classification especially under creep and irradiated conditions.

In addition, the paper discusses, as a way of code interpretation, the temperature to be used for the calculation of the material properties for plastic instability, progressive deformation, fatigue and creep fatigue checks. The temperature to be used, that is, whether local or mean depends on the failure mode being addressed.

The issue of 'secondary membrane stress' is also discussed. More work here is required to check the effect of considering the elastic DBA rules for this special case possibly at first comparing with elastoplastic analyses.

This paper, in conjunction with its companion Part I [12], provide

some detailed review of the methodologies for Elastic DBA, which is very often lacking in literature. An important conclusion is the realisation of the need to continue developing the in-house post processing script that performs Design by Elastic Analysis with minimum input from the analyst. This post processing script incorporates best practice of implementing RCC MRx elastic DBA rules to the Divertor components. The post processing script captures correct code interpretation that can be verified in-house by a number of stress analysts. With such a script, analysts can perform elastic DBA much faster and with more repeatability when compared with working through the code by performing spreadsheet program calculations. In addition, the post processing script can find more general use for components with complex geometry in other industrial applications other than nuclear fusion. A similar post processing script, specifically addressing creep – fatigue assessment was developed at the Karlsruhe Institute of Technology (KIT) [13,14].

With the availability of a reliable post processing tool, analysts can also use it to compare the elastic analysis approach with the elastic plastic approach. This would give a better understanding on the extent of how much the elastic analysis is conservative (or not) when compared to the elastic plastic approach. The elastic plastic approach is deemed to provide less conservative but still safe designs. The latter type of analysis, however, will most probably be limited because of the lack of certain material properties at different temperatures for the materials being used. In such a case, comparison can be made with limit load analyses, with elasto-plastic load analysis the latter including material softening or hardening as necessary for the Type P and Type S checks and also with shakedown theories for Type S checks.

CRediT authorship contribution statement

M. Muscat: Writing – original draft, Methodology, Investigation, Conceptualization. **P. Mollicone:** Writing – review & editing. **N. Mantel:** Writing – review & editing, Methodology, Funding acquisition, Conceptualization. **J.H. You:** Writing – review & editing, Methodology, Funding acquisition, Conceptualization. **C. Carrelli:** Methodology, Investigation. **A. Aleksa:** Methodology, Investigation. **J. Hess:** Methodology, Investigation.

Declaration of competing interest

The authors declare that they have no known competing financial interests or personal relationships that could have appeared to influence the work reported in this paper.

Acknowledgment

This work has been carried out within the framework of the EUROfusion Consortium, funded by the European Union via the Euratom Research and Training Programme (Grant Agreement No 101052200 — EUROfusion). Views and opinions expressed are however those of the author(s) only and do not necessarily reflect those of the European Union or the European Commission. Neither the European Union nor the European Commission can be held responsible for them. This work has also been part-funded by the EPSRC Energy Programme grant number EP/W006839/1.

Data availability

No data was used for the research described in the article.

References

[1] RCC-MRx, Design and construction rules for mechanical components of nuclear installations: high temperature, research and fusion reactors, AFCEN (2018).
[2] A. Aleksa, DEMO Divertor structural analyses with Global model 2022, DIV-DEMO.S.1-T017-D001 (2022), EUROfusion consortium internal report, IDM reference No. EFDA_D_2Q4BCB.
[3] J. Hess, Structural integrity assessment for shield liner and reflector plates 2022, DIV-DEMO.S.1-T017-D002 (2022), EUROfusion consortium internal report, IDM reference No. EFDA_D_2Q4BYZ.
[4] D. Marzullo, DEMO_DIVERTOR_2019 model, EUROfusion consortium internal report, IDM reference No. EFDA_D_2NCUJX v2.2.
[5] J.H. You, et al., Diverter of the European DEMO: engineering and technologies for power exhaust, Fusion Eng. Des. 175 (2022) 113010.
[6] M. Muscat, Creep-fatigue assessment tool and shakedown analysis tool, EUROfusion consortium internal report DIV-DEMO.S.4-T002-D002, IDM reference No. EFDA_D_2Q4FBT (2022).
[7] C. Carrelli, Structural integrity assessment for main Divertor EUROFER components under RCC-MRX 2022, EUROfusion consortium internal report, IDM reference No. EFDA_D_2Q478G (2022).
[8] ANSYS WorkBench, ANSYS Mechanical, Academic Research license, Release 2022 R1.
[9] EN13445-3, Unfired Pressure Vessels – Part 3: Design, CEN, 2021.
[10] ASME Boiler and Pressure vessel code, Section VIII, Division 2, Alternative rules.
[11] ASME Boiler and Pressure vessel code, Section III, Rules for construction of nuclear facility components, 2015, Division 1 – Subsection NH, Class 1 components in elevated temperature service.
[12] M. Muscat, P. Mollicone, N. Mantel, J.H. You, Insight into the structural integrity assessment of the European DEMO Fusion Reactor Divertor (Part I: general Discussion), Fusion Eng. Design 214 (2025) 114928, https://doi.org/10.1016/j.fusengdes.2025.114928. Elsevier.
[13] M. Mahler, F. Özkan, J. Aktaa, ANSYS creep-fatigue assessment tool for EUROFER97 components, Nuclear Mater. Energy 9 (2016) 535–538.
[14] M. Mahler, J. Aktaa, Eurofer97 creep-fatigue assessment tool for ANSYS APDL and workbench, Nucl. Mater. Energy 15 (2018) 85–91.